This is the accepted manuscript made available via CHORUS. The article has been published as:

Designing Ferroelectric Field-Effect Transistors Based on the Polarization-Rotation Effect for Low Operating Voltage and Fast Switching

Yubo Qi and Andrew M. Rappe

Phys. Rev. Applied **4**, 044014 — Published 21 October 2015

DOI: 10.1103/PhysRevApplied.4.044014

Low Operation Voltage Ferroelectric Field–Effect Transistor Based on Polarization Rotation Effect

Yubo Qi and Andrew M. Rappe
The Makineni Theoretical Laboratories, Department of Chemistry,
University of Pennsylvania,
Philadelphia, PA 19104-6323 USA

(Dated: September 30, 2015)

The effect of polarization rotation on the performance of metal oxide semiconductor field–effect transistors is investigated with a Landau–Ginzburg–Devonshire theory based model. In this analytical model, depolarization field, polarization rotations and the electrostatic properties of the doped silicon substrate are considered to illustrate the size effect of ferroelectric oxides and the stability of polarization in each direction. Based on this model, we provide guidance in designing electronic logic devices with low operating voltages and low active energy consumption: first, we demonstrate that MOSFET operation could be achieved by polarization reorientation with a low operating voltage, if the thickness of ferroelectric oxide is properly selected. Polarization reorientation can boost the surface potential of the silicon substrate, leading to a subthreshold swing S lower than 60 mV/decade. We also demonstrate that, compared with polarization inversion, polarization rotation offers significant advantages, including a lower energy barrier and a wider range of transferability in nano–electronic devices.

I. INTRODUCTION

Ferroelectric oxides are a promising class of materials for application in electronic devices due to their intrinsic spontaneous electric polarization, which can not only control the conductance of the channel, but also can be reoriented by an external electric field [1–4]. By modulating the polarization of ferroelectric oxides, programmable binary logic devices can be achieved, and the fast reorientation of polarization enables fast switching and lower–power operation of the metal–oxide–semiconductor field–effect transistor (MOSFET) [5, 6].

Here, we aim to provide guidance about designing a programmable fast switching MOSFET with better performance, by considering factors which were rarely included in previous modeling, but which may strongly affect the polarization reorientation and size effect of ferroelectric oxides. Many analytical models based on the Landau-Ginzburg-Devonshire (LGD) theory have been proposed previously [7, 8] to simulate the electrical behaviors of MOSFETs. These models provide an insightful understanding about the mechanisms of ferroelectric oxide based MOSFETs and guide the fabrication of novel devices. However, there are still several vital factors beyond the scope of previous models. First, the effect of the polarization distribution in three dimensions (3D) on the channel current–gate voltage relationship of a MOSFET was rarely considered, even though there were a lot of studies about polarization in 3D and its response to electric fields in different orientations [4, 9–11]. For simplicity, the polarization of the ferroelectric oxide in a MOSFET is usually treated in one dimension. Here, polarization rotation from one direction to another is the operative mode. It is true that the channel conductance is mainly modulated by the out–of–plane polarization component [12–14] and treated as in one dimension, but it is also important to note that the polarization components in all three dimensions are coupled together, and the in–plane polarization strongly influences the electric susceptibility out of plane. Furthermore, the three physical dimensions of the ferroelectric tune the relative stabilities of different local polar minima. The second factor is the electrostatic properties of the channel and gate electrode. It is widely known that the distribution of charge in electrodes, which is parameterized as screening length, determines the strength of depolarization field, which affects the magnitude of the spontaneous ferroelectric polarization [15–18].

In this letter, we propose a LGD theory based single crystal model with detailed analysis of these factors, in order to provide strategies for designing a low operation voltage ferroelectric field-effect transistor [19, 20]. A previous study argues that a subthreshold swing lower than 60 mV/decade can be achieved by the negative capacitance effect [20], but there is also debate that direct current negative capacitance is not possible, due to Gibbs free energy considerations [21]. In our model, the polarization dynamics obeys the Landau–Khalatnikov equation and is always minimizing the Gibbs free energy under a unidirectional gate voltage. We demonstrate that fast switching (subthreshold swing lower than 60 mV/decade) can be achieved by a proper design of the ferroelectric oxide size. The mechanism is that during the process of polarization reorientation, the tendency to possess spontaneous polarization in a new direction boosts the screening charge accumulation and channel current increases, leading to a low subthreshold swing.

Besides, in the polarization reorientation process, polarization rotation between in–plane and out–of–plane has a lower energy barrier compared with polarization inversion. This design aims to optimize the performance of programmable MOSFETs and can be also transferred to other electronic devices.

II. MODEL APPROACH

The LGD model is a phenomenological theory which describes the electrical properties of ferroelectric oxides. In this model, the thermodynamic potential (Gibbs free energy G_0) of a single crystal ferroelectric oxide is given as a function of polarization in three directions [22, 23].

$$\begin{aligned} G_0 &= \alpha_1 \left(P_x^2 + P_y^2 + P_z^2\right) + \alpha_{11} \left(P_x^4 + P_y^4 + P_z^4\right) \\ &+ \alpha_{12} \left(P_x^2 P_y^2 + P_y^2 P_z^2 + P_z^2 P_x^2\right) + \alpha_{111} \left(P_x^6 + P_y^6 + P_z^6\right) \\ &+ \alpha_{112} \left[P_x^4 \left(P_y^2 + P_z^2\right) + P_y^4 \left(P_z^2 + P_x^2\right) + P_z^4 \left(P_x^2 + P_y^2\right)\right] \\ &+ \alpha_{123} P_x^2 P_y^2 P_z^2 \end{aligned} \tag{1}$$

Taking external electric field and internal depolarization field into consideration, electrostatic terms should be added as

$$G = G_0 - E_x P_x - E_y P_y - E_z P_z \tag{2}$$

FIG. 1. shows the schematic of a typical MOSFET. The z axis is normal to the ferroelectric oxide/silicon interface. In the x and y directions, there is no external voltage, and short circuit conditions are applied [15, 24, 25].

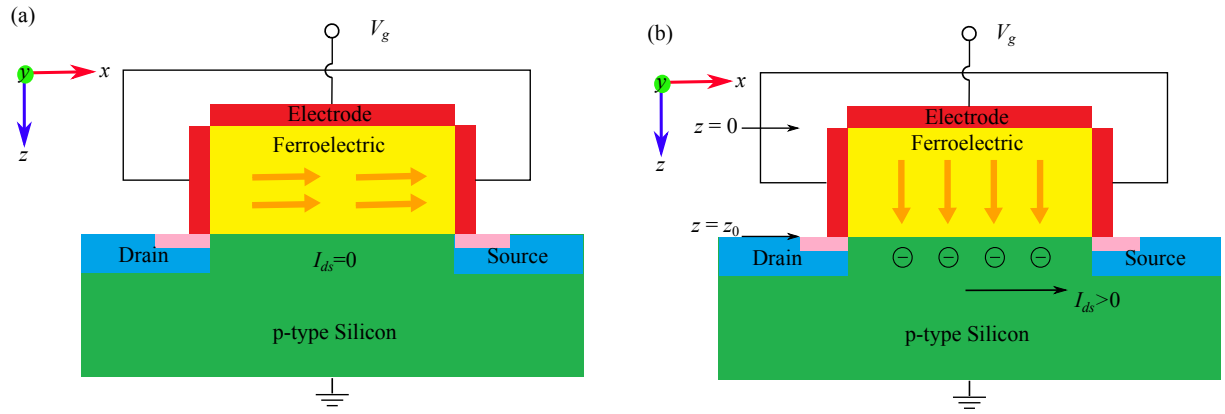

FIG. 1. The schematic of a MOSFET with ferroelectric oxide as the insulator between the gate electrode and silicon substrate. The pink rectangles represent insulator layers isolating the side electrodes and source, drain terminals. (a) No gate voltage is applied ($V_g = 0$) and the polarization is in plane. No carriers or current is in the channel; (b) Gate voltage is applied ($V_g > 0$) and polarization is out of plane. Carriers are induced by the polarization, and drain–source current flows.

For the case that a gate voltage V_g is imposed on the MOSFET, we have the following equations:

$$\left.\begin{aligned} 2V_{ex} + V_{ox} &= 0 \\ 2V_{ey} + V_{oy} &= 0 \\ V_{ez} + V_{oz} + \varphi_s &= V_g \end{aligned}\right\} \tag{3}$$

$V_{ex,ey,ez}$ and $V_{ox,oy,oz}$ are the voltage drop across the electrode and the ferroelectric oxide in the x, y and z directions. φ_s is the surface potential of the silicon substrate, and it can also be viewed as the voltage drop in the doped silicon substrate. The flat band potential V_{fb}, which results from the alignment of the Fermi levels of the gate electrode, oxide, and silicon substrate is included in V_g. The electric field $\boldsymbol{E}$ is determined by both the external applied voltage and the electrostatic properties of the ferroelectric oxide and electrodes [26–28]. It is widely accepted that the charge density in noble metal electrodes follows the Thomas-Fermi distribution, and this distribution causes a voltage drop across the electrodes. The following derivation calculating this potential drop follows the main idea in Ref. 24, but is re–interpreted. Taking the z direction as an example (the electrostatic properties in the x, y directions following similar rules), the relationship between the electric field and the charge density takes the form

$$\frac{dE(z)}{dz} = -\frac{Q(z)}{\varepsilon_0 \varepsilon_e} = -q\frac{n(z) - n_0}{\varepsilon_0 \varepsilon_e} \tag{4}$$

$E(z)$, $Q(z)$ and $n(z)$ are the electric field, the charge density and the electron density in electrodes at the position z. n_0 is the average electron density in a neutral electrode. q is the electronic charge. ε_0 and ε_e are the electric permittivities of the vacuum and electrode. Meanwhile, the potential drop $V(z)$ is expressed as

$$\frac{dV(z)}{dz} = -E(z) \quad \Longrightarrow \quad \frac{dV(z)}{dn(z)}\frac{dn(z)}{dz} = -E(z) \tag{5}$$

The electrons in metal electrodes are treated as a free Fermi gas, so the local potential and the electron density are related as [29]

$$V = \frac{\hbar^2}{2m}\left(3\pi^2 n\right)^{\frac{2}{3}} \tag{6}$$

$$\frac{dV(z)}{dn(z)} = \frac{\hbar^2}{3m}\left(3\pi^2\right)^{\frac{2}{3}} n(z)^{-\frac{1}{3}} \tag{7}$$

$\hbar$ is the reduced Planck constant and m is the electronic mass. By combining equations (5) and (7), we have

$$\frac{dn(z)}{dz} = -\left[\frac{\hbar^2}{3m}\left(3\pi^2\right)^{\frac{2}{3}} n(z)^{-\frac{1}{3}}\right]^{-1} E(z) \tag{8}$$

Taking the derivative of equation (4), we have

$$\frac{d^2E(z)}{dz^2} = -\frac{q}{\varepsilon_0\varepsilon_e}\frac{dn(z)}{dz} = \frac{3mq}{\varepsilon_0\varepsilon_e\hbar^2}\left(3\pi^2\right)^{-\frac{2}{3}} n(z)^{\frac{1}{3}} E(z) \tag{9}$$

The characteristic length λ_z (in the z direction, and later we will introduce λ_x and λ_y as the characteristic length in the x and y directions), which is also called screening length and determines the dispersion of electrons in electrodes, is defined as

$$\lambda_z^2 = \left[\frac{3mq}{\varepsilon_0\varepsilon_e\hbar^2}\left(3\pi^2\right)^{-\frac{2}{3}} n(z)^{\frac{1}{3}}\right]^{-1} \approx \left[\frac{3mq}{\varepsilon_0\varepsilon_e\hbar^2}\left(3\pi^2\right)^{-\frac{2}{3}} n_0^{\frac{1}{3}}\right]^{-1} \tag{10}$$

Here, we take the approximation that in a metallic material, the electron density at any position is approximately the same as the background one. Therefore, λ_z is regarded as a constant and equation (9) is rewritten as

$$\frac{d^2E(z)}{dz^2} = \frac{1}{\lambda_z^2}E(z) \tag{11}$$

The boundary conditions are

$$\begin{cases} E(0) = \dfrac{Q(z=0)}{\varepsilon_0\varepsilon_e} \\ \\ E(-\infty) = 0 \end{cases} \tag{12}$$

$Q(z=0)$ is the screening charge density at the ferroelectric/oxide electrode interface, which is perpendicular to the z direction. Thus, the electric field and potential drop through one electrode are

$$E(z) = \frac{Q(z=0)}{\varepsilon_0\varepsilon_e}e^{z/\lambda_z} \tag{13}$$

$$V_e = \int_{-\infty}^{0} E(z)\,dz = \int_{-\infty}^{0} \frac{Q(z=0)}{\varepsilon_0\varepsilon_e}e^{z/\lambda_z}dz = \frac{Q(z=0)\lambda_z}{\varepsilon_0\varepsilon_e} \tag{14}$$

The heterostructure of electrode, ferroelectric oxide, and silicon substrate can be regarded as a capacitor, with equal magnitude of charge densities at each interface:

$$Q(z=0) = -Q(z=z_0) \tag{15}$$

where z_0 is the position of the interface between the silicon substrate and ferroelectric oxide. However, the charge distribution in the doped silicon substrate is quite different from that in metal. This is because electrons in the metal are treated as a free electron gas. This is the basic approximation of the Thomas-Fermi model. But doped silicon is a semiconductor, and the free carrier density is local potential dependent [30, 31]. The interface charge density–potential relationship in the silicon substrate is given by

$$Q(z=0) = \sqrt{2\varepsilon_{Si}kTN_a}\cdot\left[\left(e^{-\frac{q\varphi_s}{kT}} + \frac{q\varphi_s}{kT} - 1\right) + \frac{n_i^2}{N_a^2}\left(e^{\frac{q\varphi_s}{kT}} - \frac{q\varphi_s}{kT} - 1\right)\right]^{\frac{1}{2}} \tag{16}$$

$$\frac{d\varphi(z)}{dz} = E(z) = \sqrt{\frac{2kTN_a}{\varepsilon_{Si}}}\cdot\left[\left(e^{-\frac{q\varphi(z)}{kT}} + \frac{q\varphi(z)}{kT} - 1\right) + \frac{n_i^2}{N_a^2}\left(e^{\frac{q\varphi(z)}{kT}} - \frac{q\varphi(z)}{kT} - 1\right)\right]^{\frac{1}{2}} \tag{17}$$

φ_s is the surface potential of the silicon substrate. k is the Boltzmann constant. Other parameters are listed and described in TABLE I.

From the analysis above, we see that the charge density decreases gradually away from the oxide in both the metal electrode and the doped silicon substrate, even though the analytical expressions and physical mechanisms which govern the charge distribution are different. As a result, there are voltage drops through each layer. These voltage drops could counteract or completely neutralize the applied gate voltage, exerting significant influence on the magnitudes of ferroelectric polarization and charge in the channel. Equation (16) demonstrates that there is a

one–to–one correlation between the interface charge density $Q(z=0)$ and the surface potential at $z=z_0$ φ_s. φ_s is a function of $Q(z=0)$:

$$\varphi_s = f\left[Q(z=0)\right] \tag{18}$$

The voltage drop across the ferroelectric oxide takes the form

$$V_{oz} = E_z \cdot d_z = \frac{Q(z=0) - P_z}{\varepsilon_0} d_z \tag{19}$$

d_z is the thickness of the ferroelectric film and P_z is the polarization in the z direction. With the analysis above, equation set (3) is rewritten as

$$\left.\begin{aligned} &2\frac{Q(x=0)\lambda_x}{\varepsilon_0\varepsilon_e} + \frac{Q(x=0)-P_x}{\varepsilon_0} d_x = 0 \\ &2\frac{Q(y=0)\lambda_y}{\varepsilon_0\varepsilon_e} + \frac{Q(y=0)-P_y}{\varepsilon_0} d_y = 0 \\ &\frac{Q(z=0)\lambda_z}{\varepsilon_0\varepsilon_e} + \frac{Q(z=0)-P_z}{\varepsilon_0} d_z + f\left[Q(z=0)\right] = V_g \end{aligned}\right\} \tag{20}$$

For short–circuit conditions, in order to balance the potential drop in the electrodes, the sign of $V_{ox,oy}$ should be opposite to that of $V_{ex,ey}$. This indicates that surface charge density should be smaller than polarization, which means an incomplete screening of the polarization charge. As a result, an electric field (depolarization field) is induced opposite to the polarization. The potential drop in the metal electrodes, which is proportional to screening length, is the origin of the incomplete polarization charge screening and the depolarization field which suppresses ferroelectricity.

The energy surface versus polarization direction and magnitude can be plotted under the electrostatic restrictions expressed in equation (20). After acquiring the energy surface, polarization dynamics on the energy surface is simulated by the Landau–Khalatnikov equation [32–34],

$$\gamma \frac{d\overrightarrow{P}}{dt} + \nabla_{\overrightarrow{P}} G = 0 \tag{21}$$

γ is the polarization dynamic parameter. G is the thermodynamic potential defined in equation (2) with the restriction shown in equation (20). The most stable polarization is the one which minimizes Gibbs free energy G. However, if the polarization is not in a local minimum, it cannot move to one instantaneously. The rate of return to a minimum is determined by many factors. For example, the resistance of the circuits affects this rate, because polarization evolution must be accompanied by screening charge transmission; The speed of domain wall motion is also a key factor, because polarization reorientation is accompanied with the nucleation and growth of a new domain [35, 36]. The polarization dynamic parameter γ is related to the mobility of polarization, as $\nabla_{\overrightarrow{P}} G$ can be regarded as the driving force of polarization and $\gamma \frac{d\overrightarrow{P}}{dt}$ is the speed of polarization evolution. The applied time–varying gate voltage takes the form,

$$V_g = V_0 \sin(\omega t) \qquad \left(0 < t < \frac{\pi}{\omega}\right) \tag{22}$$

Here, we do not mean that the applied gate voltage is oscillatory. Instead, we are simulating one on/off programmable cycle $\left(0 < t < \frac{\pi}{\omega}\right)$, and the increase/decrease of the gate voltage takes the sine form. Equation (21) is rewritten as

$$\gamma_0 \frac{d\overrightarrow{P}}{d(\omega t)} + \nabla_{\overrightarrow{P}} G = 0 \tag{23}$$

$\gamma_0 = \omega\gamma$ is the effective polarization dynamic parameter. φ_s and $Q(z=0)$ can be calculated from P_z and the drain-source current I_{ds} is obtained by the Pao-Sah double integral [37].

$$I_{ds} = q\mu_{\text{eff}} \frac{W}{L} \int_0^{V_{ds}} \left(\int_\delta^{\varphi_s} \frac{\frac{n_i^2}{N_a} e^{q(\varphi - V)/kT}}{E(\varphi, V)} d\varphi \right) dV \tag{24}$$

where the function $E(\varphi, V)$ is the electric field in the channel as given in Ref. [31]. δ is an infinitesimal quantity. All the parameters in this simulation are listed in TABLE I.

TABLE I. PARAMETERS INVOLVED IN THIS STUDY

	Description	Value
T	Temperature	298 K
α_1	Coefficient in LGD theory[a]	-2.77×10^7 m/F
α_{11}	Coefficient in LGD theory[a]	-5.35×10^8 m^5/C^{2}F
α_{12}	Coefficient in LGD theory[a]	3.23×10^8 m^5/C^{2}F
α_{111}	Coefficient in LGD theory[a]	8.00×10^9 m^9/C^{4}F
α_{112}	Coefficient in LGD theory[a]	4.47×10^9 m^9/C^{4}F
α_{123}	Coefficient in LGD theory[a]	4.91×10^9 m^9/C^{4}F
$\lambda_{x,y,z}$	Screening lengths in noble metal[b]	0.04 nm
ε	Dielectric constant of noble metal[b]	2.0
N_a	Substrate doping concentration[c]	4×10^{15} cm^{-3}
n_i	Intrinsic carrier concentration[c]	1.5×10^{11} cm^{-3}
ε_{Si}	Dielectric constant of silicon	11.7 F/m
μ_{eff}	Effective electron mobility	3.0×10^{-2} m^2/Vs
W	Width of the silicon channel	4.0×10^{-7} m
L	Length of the silicon channel	4.0×10^{-7} m
d_y	Equal to d_x	

[a] Reference [22]
[b] Reference [28]
[c] Reference [31]

III. RESULTS AND ANALYSIS

The ferroelectric oxide we choose is $BaTiO_3$, which possesses a relatively large spontaneous polarization ($P_s \approx 0.26$ C/m^2) at room temperature [17].

In order to simulate the energy surface, we vary the surface potential φ_s and polarization P_x. For each φ_s, charge density $Q(z=0)$ and polarization P_z are determined uniquely by equations (16) and (20). At room temperature, the $BaTiO_3$ crystal has a tetragonal phase. The polarization orients either out of plane or in plane. We set the in–plane polarization direction as the x direction and $P_y = 0$. Here, we should also note that we assume that the in–plane polarization has no effect on the channel. Therefore, it is not necessary that the source channel–drain–current flows along the x direction. Electric field $\boldsymbol{E}$ is obtained by the electrostatic restrictions in equation (20). Then energy surfaces describing Gibbs free energy G with respect to P_x and P_z are calculated by formula (1) and (2).

In FIG. 2, we have plotted two energy surfaces of $BaTiO_3$ with different thicknesses in the x and z directions on a p–type silicon substrate.

From the graphs, we can see that for out–of–plane polarization, a negative orientation (pointing to gate electrode, with negative ends of oxide dipoles toward the channel) is more favorable when there is no applied voltage. This is because for a p–type silicon substrate, positive screening charge is more likely to accumulate at the interface, leading to the polarization pointing away from the substrate/ferroelectric oxide interface. FIG. 3 shows the relationship of the surface potential and the interface charge density in the p–type silicon substrate. A positive (pointing to silicon substrate) spontaneous polarization $P_{z+} \approx 0.26$ C/m^2 corresponds to a surface potential $\varphi_s = 0.962$ eV, while $P_{z-} \approx -0.26$ C/m^2 corresponds to a surface potential $\varphi_s = -0.4346$ eV. The depolarization fields through the ferroelectric oxide are calculated with the equation (20):

$$E_z = \frac{1}{d_z}\left[V_g - f\left(Q\left(z=0\right)\right) - \frac{Q\left(z=0\right)\lambda_z}{\varepsilon_0\varepsilon_e}\right] \tag{25}$$

$$\left|E_z\left(P_{z+}\right)\right| = \frac{1}{d_z}\left[0.962 + \frac{0.26\lambda_z}{\varepsilon_0\varepsilon_e}\right] > \left|E_z\left(P_{z-}\right)\right| = \frac{1}{d_z}\left[0.4346 + \frac{0.26\lambda_z}{\varepsilon_0\varepsilon_e}\right] \tag{26}$$

The depolarization field for positive polarization is larger, and this explains why on the energy surface with no gate voltage, a negative polarization is more favorable than a positive one.

Besides, the graphs also demonstrate the known relation that the thicker the ferroelectric oxide is in one direction, the more stable the polarization in this direction. As shown in equation (20), if the thickness overwhelms the screening length, the potential drop in the electrodes can be neglected [38]. As a result, the electric field through the ferroelectric oxide decreases, making the polarization in this direction more favorable.

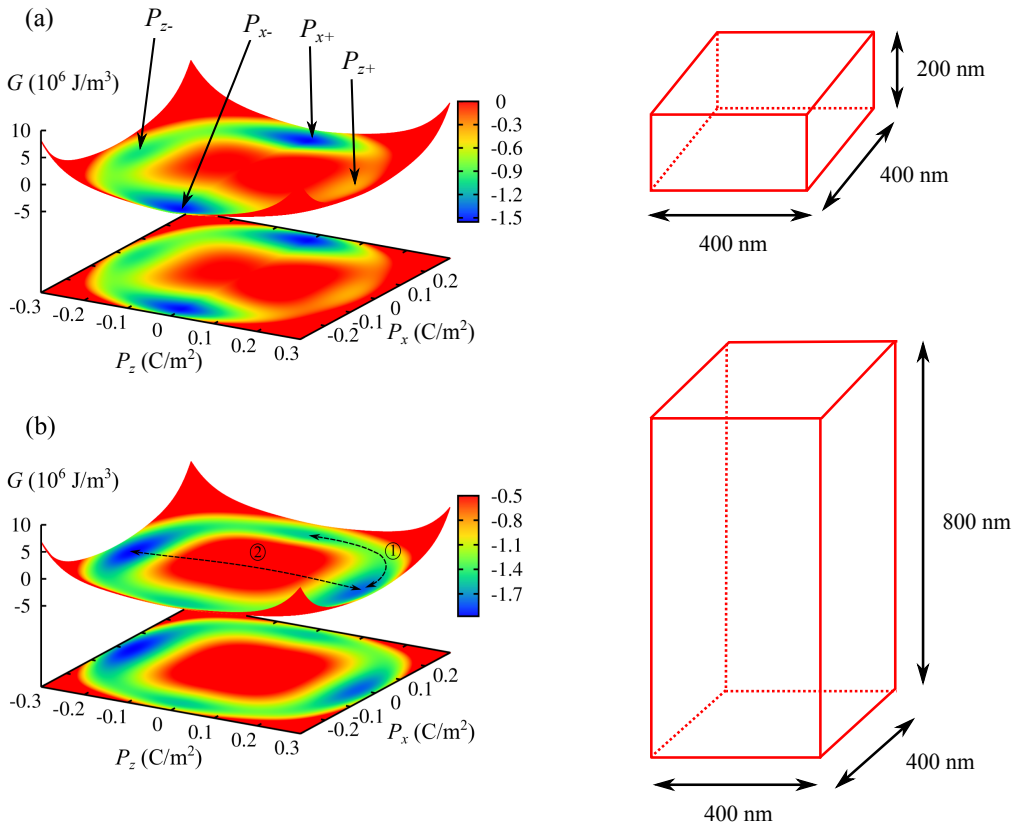

FIG. 2. Energy surfaces and their two dimensional projections for MOSFET systems with ferroelectric oxide $BaTiO_3$ of different sizes. Parameters used in the simulation are given in Ref. [22]. (*a*) $d_x = 400$ nm and $d_z = 200$ nm, polarization in plane favored. Polarizations corresponding to the four local minima are marked as P_{x+}, P_{x-}, P_{z+} and P_{z-}; (*b*) $d_x = 400$ nm and $d_z = 800$ nm, polarization out of plane favored. Polarization dynamics is marked with the dashed lines, path 1: polarization rotation; path 2: polarization inversion.

These results also illustrate that we can modulate the global minimum by adjusting the three-dimensional size of the ferroelectric oxide. An energy surface we are particularly interested in possesses the global minimum for P_x. When the gate voltage is applied, the local minimum corresponding to P_{z+} becomes deeper and polarization rotates to the z direction. After the gate voltage is turned off, the polarization relaxes back along the x direction. Meanwhile, the depth of the local minimum for P_{z+} is close to that for P_x. In such a situation, a relatively small applied gate voltage V_g could induce polarization to rotate from the x direction to the z direction. The channel current strongly depends on the interface charge density, which is approximately equal to the polarization in the z direction.

$$I_{ds} \xrightarrow{\text{depends on}} Q\left(z=0\right) \approx P_z \tag{27}$$

Here, we provide guidance about how to select the optimal widths of the ferroelectric oxide, in order to make the polarization rotation likely to occur. First, in order to make the polarization orient in the x direction without gate voltage, the depolarization field for P_x should be smaller than the one that corresponds to P_{z-},

$$|E_x| = \frac{1}{d_x}\left|\frac{2\times 0.26\lambda_x}{\varepsilon_0\varepsilon_e}\right| < |E_z\left(P_{z-}\right)| = \frac{1}{d_z}\left[0.4346 + \frac{0.26\lambda_z}{\varepsilon_0\varepsilon_e}\right] \tag{28}$$

Typically, the dielectric constant and screening length of the noble metal electrodes are $\varepsilon_e = 2$ and λ =0.4 Å [28]. For these values, we have the criterion

$$\frac{d_z}{d_x} < 0.87 \tag{29}$$

In order to have a programmable device, when the applied gate voltage V_g returns 0, the polarization should spontaneously return from the P_{z+} position to the minimum for P_x on the energy surface. According to the Landau–

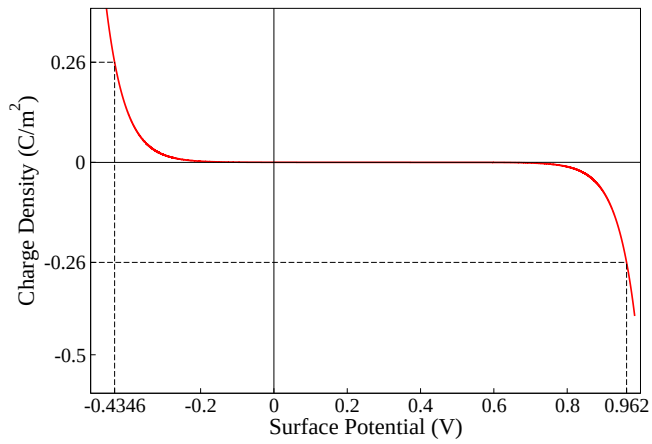

FIG. 3. The relationship of surface potential and interface charge density in the doped silicon substrate. Positive polarization (negative screening charge) corresponds to a larger surface potential and depolarization field.

Khalatnikov equation, the P_{z+} position on the energy surface should be a saddle point,

$$\frac{\partial^2 G}{\partial {P_x}^2} < 0 \bigg|_{P_z = P_{z+}} \implies \alpha_1 + \alpha_{12} P_{z+}^2 + \alpha_{112} P_{z+}^4 + \frac{2\lambda_x}{d_x \varepsilon_0 \varepsilon_e} < 0 \tag{30}$$

The value of P_{z+} increases with thickness in the z direction, since a thinner film means a larger depolarization field which suppresses the ferroelectr

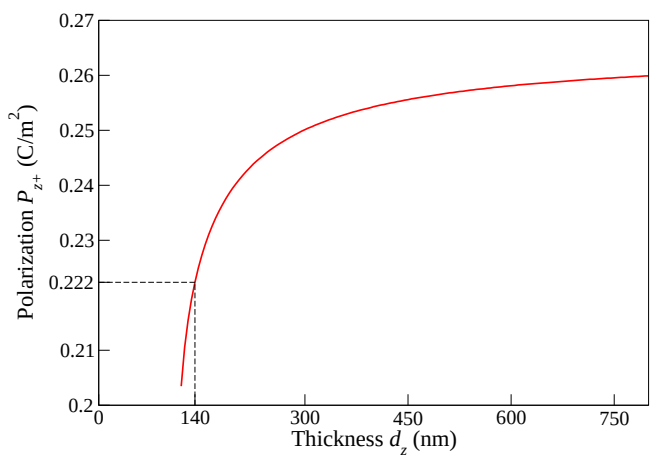

FIG. 4. The P_{z+} vs. d_z plot. Only when the thickness in the z direction d_z is below 140 nm, P_{z+} is smaller than 0.223 C/m^2.

$$\alpha_1 + \alpha_{12} P_{z+}^2 + \alpha_{112} P_{z+}^4 < 0 \Rightarrow 0 < P_{z+} < 0.223 \text{ C/m}^2 \tag{31}$$

Therefore $d_z < 140$ nm is a necessary condition for the polarization rotating back to the x direction.

$$\alpha_1 + \frac{2\lambda_x}{d_x \varepsilon_0 \varepsilon_e} < 0 \Rightarrow d_x > 167 \text{ nm} \tag{32}$$

According to the analysis above, in this study, the $BaTiO_3$ dimensions are selected as $d_x = 400$ nm and $d_z = 100$ nm.

Hysteresis loops with different values of γ_0 are calculated and shown in FIG. 5. It demonstrates that if γ_0 is too large, the out–of–plane polarization cannot reduce to 0 and the device is not ready for the next program cycle. From our simulation, the threshold γ_0 for out–of–plane polarization returning to 0 completely is around 1.0×10^5 m/F. γ_0 is not only frequency dependent as shown in equation (23), but also dependent on the resistance in the circuit [39, 40],

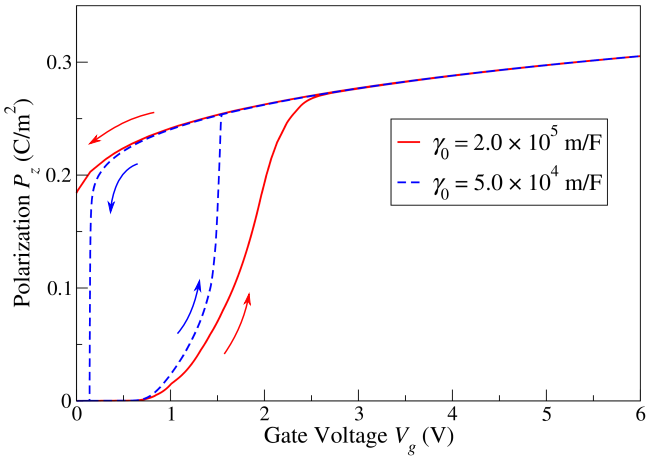

FIG. 5. Hysteresis loop of the out–of–plane polarization P_z, with different values of γ_0.

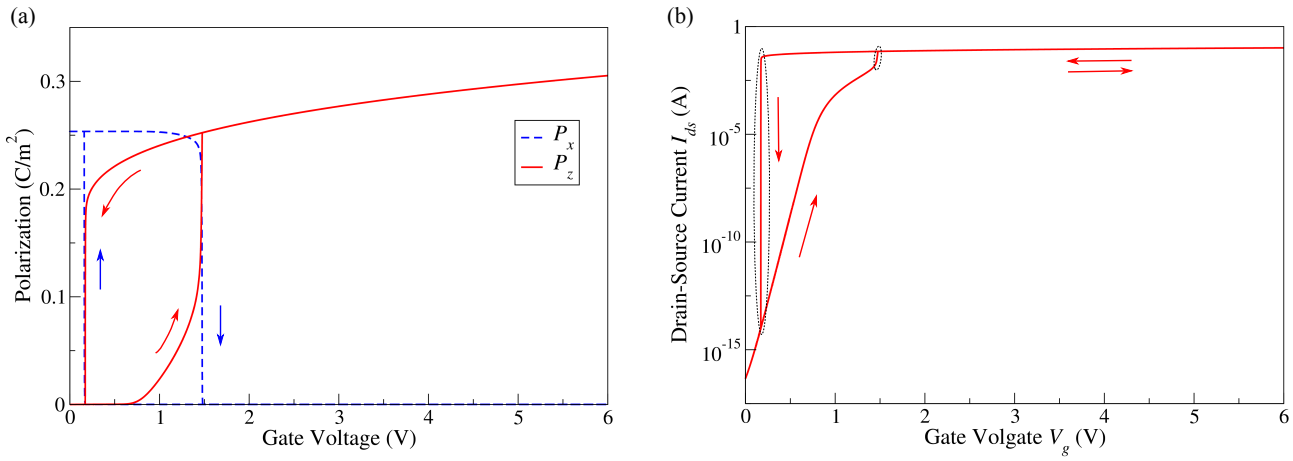

FIG. 6. (a) Hysteresis loop of the in–plane polarization P_x and out–of–plane polarization P_z, effective polarization dynamic parameter $\gamma_0 = 1.0 \times 10^4$ m/F; (b) $I_{ds} - V_g$ curve of MOSFET. In the circled part, the inverse slope swing is lower than 60 mV/decade.

since polarization dynamics is accompanied by screening charge transmission [28, 41]. Therefore, in order to make γ_0 in the acceptable range and to have a short switching time, the resistance in the circuit should be low.

To evaluate the performance of MOSFET, The drain–source current I_{ds} and gate voltage V_g relationship is calculated based on Pao–Sah double integral. The simulated hysteresis loop and $I_{ds} - V_g$ curve for $\gamma_0 = 1.0 \times 10^4$ m/F are shown in FIG. 6 (b).

From the simulation, it can be seen that the on/off ratio of the channel current is large, which means that this device is extremely suitable for logic technology. This large on/off ratio results from spontaneous polarization rotation, because the spontaneous polarization attracts screening charge as free carriers, leading to a large on–current. The segments in the $I_{ds} - V_g$ curve circled by dashed lines possess subthreshold swings S lower than 60 mV/decade. For the segment with I_{ds} and V_g increasing, $S = 53$ mV/decade, and the S of the decreasing segment is even lower. This is because, as the gate voltage V_g increases and exceeds the threshold voltage, the polarization rotates and boosts free carriers in the silicon channel, inducing a steep increase of the channel current. From FIG. 6, we can see that the steep change of the channel current is accompanied by polarization reorientation.

S can be expressed as [20]

$$S = \frac{\partial V_g}{\partial \left(\log_{10} I_{ds}\right)} = \frac{\partial V_g}{\partial \varphi_s} \frac{\partial \varphi_s}{\partial \left(\log_{10} I_{ds}\right)} \tag{33}$$

FIG. 7 shows the potential diagrams along the z direction of top electrode/ferroelectric oxide/bottom electrode systems at 0 applied gated voltage [42]. During the polarization reorientation period, the polarization changes suddenly from

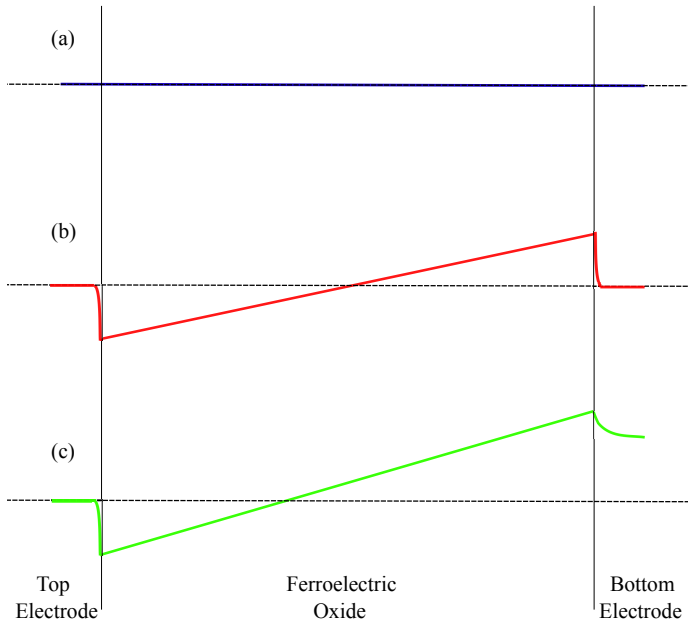

FIG. 7. Potential diagrams of the systems with (a) polarization in the plane, so that in the z direction the ferroelectric oxide is essentially a normal dielectric material; (b) polarization out of plane and both electrodes are noble metals; (c) polarization out of plane. The top electrode is noble metal and the bottom one is doped silicon substrate. The potential should decay to 0. For simplicity, the curve truncates at 2 nm from the oxide/silicon interface.

an in–plane one corresponding to zero surface potential to a positive out–of–plane polarization, which maintains a large surface potential as demonstrated in FIGs. 3 and 7. The surface potential is boosted as

$$\frac{\partial V_g}{\partial \varphi_s} < 1, \tag{34}$$

causing S to break the 60 mV/decade limit.

Compared with polarization inversion, polarization rotation possesses many advantages for electronic device applications. First, as shown in FIG. 2, the polarization rotation process encounters a much lower energy barrier, leading to a lower polarization rotation voltage [43] and a smaller polarization dynamic parameter. Besides, this design is quite suitable for programmable electronic devices. Like the traditional SiO_2 based MOSFET, channel current is turned off under the removal of the gate voltage. Thus, there should not be a local minimum for P_{z+}. d_z must be small ($<$ 140 nm) so that the depolarization field in the z direction is large. For the polarization inversion case, the local minimum for P_{z-} should be deeper than that for P_{x+} or P_{x-}, which requires a d_x with nearly the same dimension as d_z. Such a smaller scale oxide sets a much higher requirement for fabrication. Also, the working state of the MOSFET can be modulated by a unidirectional gate voltage, by just the application and removal, rather than flipping the direction. What is more, this simulation and the guidance about designing the ferroelectric oxide size can be extended to other types of channel, such as quantum wells, granular films and graphene [6, 44–48]. The only aspect that must be modified according to the electric properties of new channels is the surface potential–interface charge density relationship

$$\varphi_s = f\left[Q\left(z=0\right)\right] \tag{35}$$

Recently, a granular film based electric field sensor system has been systematically investigated [45]. This novel device design has a wide range of potential application in electric–field sensors, temperature sensors and memory cells. For the granular film, both positive and negative out–of–plane polarization can induce screening charge in metallic grains and enhance the conductivity. Therefore, our polarization rotation design also has significance in modulating such devices. The graphene sensor is a similar case [46]: out–of–plane polarization in any direction can shift the Fermi level away from the Dirac point and make the channel conductive. Polarization rotation could be an effective method to turn on/off the channel current.

In this paper, the focus is $BaTiO_3$, but this analytical model can also be applied to other ferroelectric oxides, such as $PbTiO_3$ and $PbZr_{1-x}Ti_xO_3$. $PbTiO_3$ possesses a larger energy barrier in the polarization process compared with $BaTiO_3$ [49]. Therefore, a larger applied gate voltage would be needed, or we could use $PbTiO_3$ with smaller

dimensions. Also, a single–domain ferroelectric oxide is assumed in this model. However, the effect is not limited to a single crystal. When a gate voltage is applied, polarization in the z direction increases in different grains and finally the polarization becomes approximately uniform. After the voltage is removed, the polarization relaxes back to the plane. Multiple domains may form in each grain, but the polarization distribution in plane has little effect on the channel conductance.

IV. CONCLUSION

In summary, the polarization distribution in 3D and the electrical properties of the electrodes and the silicon substrate were highlighted in this LGD–theory–based model. Our model demonstrated that polarization reorientation can modulate the drain–source current effectively. Besides, the choice of electrodes and the dimensions of the ferroelectric oxide are key factors in determining the performance of a MOSFET with depolarization fields. With proper selection of the thicknesses, field effect transistor with low operating voltage and fast switching ($S < 60$ mV/decade) can be achieved by the polarization reorientation of the ferroelectric oxide.

ACKNOWLEDGMENTS

Y. Q. would like to acknowledge the support of the National Science Foundation, under Grant No. DMR1124696. A. M. R. acknowledges the support of the Department of Energy, under Grant No. DE–FG02–07ER15920. Both authors thank the National Energy Research Scientific Computing Center for their computational support. The authors thank Jonathan E. Spanier for productive discussions about this work.

[1] S. Mathews, R. Ramesh, T. Venkatesan, and J. Benedetto, Ferroelectric field effect transistor based on epitaxial perovskite heterostructures, Science **276**, 238 (1997).
[2] R. C. Naber, C. Tanase, P. W. Blom, G. H. Gelinck, A. W. Marsman, F. J. Touwslager, S. Setayesh, and D. M. De Leeuw, High–performance solution–processed polymer ferroelectric field–effect transistors, Nat. Mater. **4**, 243 (2005).
[3] J. Hoffman, X. Pan, J. W. Reiner, F. J. Walker, J. Han, C. H. Ahn, and T. Ma, Ferroelectric field effect transistors for memory applications, Adv. Mater. **22**, 2957 (2010).
[4] H. Fu and R. E. Cohen, Polarization rotation mechanism for ultrahigh electromechanical response in single–crystal piezoelectrics, Nature **402**, 281 (2000).
[5] H. Kimura, T. Hanyu, M. Kameyama, Y. Fujimori, T. Nakamura, and H. Takasu, Complementary ferroelectric–capacitor logic for low–power logic–in–memory VLSI, IEEE J. Solid-State Circuits **39**, 919 (2004).
[6] L. Liu, V. Narayanan, and S. Datta, A programmable ferroelectric single electron transistor, Appl. Phys. Lett. **102**, 053505 (2013).
[7] Y. Chen, Y. En, Y. Huang, X. Kong, W. Fang, and X. Zheng, Effects of stress and depolarization on electrical behaviors of ferroelectric field–effect transistor, IEEE Electron Device Lett. **33**, 110 (2012).
[8] H.-P. Chen, V. C. Lee, A. Ohoka, J. Xiang, and Y. Taur, Modeling and design of ferroelectric MOSFETs, IEEE Trans. Electron Devices **58**, 2401 (2011).
[9] L. Bellaiche, A. Garcia, and D. Vanderbilt, Heterovalent and A-atom effects in A(B'B")O_3 perovskite alloys, Phys. Rev. B Rapid Comm. **64**, 060103(R) (2001).
[10] J. Hlinka and Márton, Phenomenological model of a 90° domain wall in $BaTiO_3$–type ferroelectrics, Phys. Rev. B. **74**, 104104 (2006).
[11] V. Nagarajan, A. Roytburd, A. Stanishevsky, S. Prasertchoung, T. Zhao, L. Chen, J. Melngailis, O. Auciello, and R. Ramesh, Dynamics of ferroelastic domains in ferroelectric thin films, Nat. Mat. **2**, 43 (2002).
[12] C. H. Ahn, A. Bhattacharya, M. Di Ventra, J. N. Eckstein, C. D. Frisbie, M. E. Gershenson, A. M. Goldman, I. H. Inoue, J. Mannhart, A. J. Millis, F. Morpurgo, Alberto, D. Natelson, and J.-M. Triscone, Electrostatic modification of novel materials, Rev. Mod. Phys. **78**, 1185 (2006).
[13] K. S. Takahashi, M. Gabay, D. Jaccard, K. Shibuya, T. Ohnishi, M. Lippmaa, and J.-M. Triscone, Local switching of two–dimensional superconductivity using the ferroelectric field effect, Nature **441**, 195 (2006).
[14] N. Reyren, S. Thiel, A. D. Caviglia, L. F. Kourkoutis, G. Hammerl, C. Richter, C. W. Schneider, T. Kopp, A. S. Rüetschi, D. Jaccard, M. Gabay, D. A. Muller, J.-M. Triscone, and J. Mannhart, Superconducting interfaces between insulating oxides, Science **317**, 1196 (2007).
[15] I. Batra, P. Wurfel, and B. Silverman, Phase transition, stability, and depolarization field in ferroelectric thin films, Phys. Rev. B **8**, 3257 (1973).
[16] N. Sai, A. M. Kolpak, and A. M. Rappe, Ferroelectricity in ultra–thin perovskite films, Phys. Rev. B Rapid Comm. **72**, 020101(R) (2005).

[17] W. A. Al-Saidi and A. M. Rappe, Density functional study of $PbTiO_3$ nanocapacitors with Pt and Au electrode, Phys. Rev. B **82**, 155304 (2010).

[18] M. A. Mendez-Polanco, I. Grinberg, A. M. Kolpak, S. V. Levchenko, C. Pynn, and A. M. Rappe, Stabilization of highly polarized $PbTiO_3$ nanoscale capacitors due to in–plane symmetry breaking at the interface, Phys. Rev. B **85**, 214107 (2012).

[19] S. Datta, R. Bijesh, H. Liu, D. Mohata, and V. Narayanan, Tunnel transistors for energy efficient computing, *Reliability Physics Symposium (IRPS), 2013 IEEE International* (IEEE, 2013) pp. 6A–3.

[20] S. Salahuddin and S. Datta, Use of negative capacitance to provide voltage amplification for low power nanoscale devices, Nano. Lett. **8**, 405 (2008).

[21] C. Krowne, S. Kirchoefer, W. Chang, J. Pond, and L. Alldredge, Examination of the possibility of negative capacitance using ferroelectric materials in solid state electronic devices, Nano. Lett. **11**, 988 (2011).

[22] N. A. Pertsev, A. G. Zembilgotov, and A. K. Tagantsev, Effect of mechanical boundary conditions on phase diagrams of epitaxial ferroelectric thin films, Phys. Rev. Lett. **80**, 1988 (1998).

[23] V. G. Koukhar, N. A. Pertsev, and R. Waser, Thermodynamic theory of epitaxial ferroelectric thin films with dense domain structures, Phys. Rev. B **64**, 214103 (2001).

[24] R. R. Mehta, B. D. Silverman, and J. T. Jacobs, Depolarization fields in thin ferroelectric films, J. Appl. Phys. **44**, 3379 (1973).

[25] A. M. Kolpak, N. Sai, and A. M. Rappe, Short–circuit boundary conditions in ferroelectric $PbTiO_3$ thin films, Phys. Rev. B **74**, 054112 (2006).

[26] P. Wurfel and I. P. Batra, Depolarization–field–induced instability in thin ferroelectric films—experiment and theory, Phys. Rev. B **8**, 5126 (1973).

[27] J. Junquera and P. Ghosez, Critical thickness for ferroelectricity in perovskite ultrathin films, Nature **422**, 506 (2003).

[28] D. Kim, J. Jo, Y. Kim, Y. Chang, J. Lee, J.-G. Yoon, T. Song, and T. Noh, Polarization relaxation induced by a depolarization field in ultrathin ferroelectric $BaTiO_3$ capacitors, Physical review letters **95**, 237602 (2005).

[29] C. kittel, *Introduction to Solid State Physics*, Vol. 7 (John Wiley & Sons, 1971) p. 247.

[30] S. M. Sze and K. K. Ng, *Physics of semiconductor devices* (John Wiley & Sons, 2006).

[31] Y. Taur, T. H. Ning, *et al.*, *Fundamentals of modern VLSI devices*, Vol. 2 (Cambridge University Press Cambridge, 1998).

[32] L. Landau and I. Khalatnikov, in *Dokl. Akad. Nauk SSSR*, Vol. 96 (1954) pp. 469–472.

[33] V. C. Lo, Simulation of thickness effect in thin ferroelectric films using Landau–Khalatnikov theory, J. Appl. Phys. **94**, 3353 (2003).

[34] W. Zhang and K. Bhattacharya, A computational model of ferroelectric domains. Part I: model formulation and domain switching, Acta Mater. **53**, 185 (2005).

[35] Y.-H. Shin, I. Grinberg, I.-W. Chen, and A. M. Rappe, Nucleation and growth mechanism of ferroelectric domain–wall motion, Nature **449**, 881 (2007).

[36] R. Xu, S. Liu, I. Grinberg, J. Karthik, A. R. Damodaran, A. M. Rappe, and L. W. Martin, Ferroelectric polarization reversal via successive ferroelastic transitions, Nat. Mater. **14**, 79 (2015).

[37] H. C. Pao and C.-T. Sah, Effects of diffusion current on characteristics of metal–oxide (insulator)–semiconductor transistors, Solid-State Electronics **9**, 927 (1966).

[38] J. E. Spanier, A. M. Kolpak, J. J. Urban, I. Grinberg, L. Ouyang, W. S. Yun, A. M. Rappe, and H. Park, Ferroelectric phase transition in individual single–crystalline $BaTiO_3$ nanowires, Nano Lett. **6**, 735 (2006).

[39] S. Sivasubramanian, A. Widom, and Y. Srivastava, Equivalent circuit and simulations for the Landau–Khalatnikov model of ferroelectric hysteresis, Ultrasonics, Ferroelectrics and Frequency Control, IEEE Transactions on **50**, 950 (2003).

[40] Y. Zhou, H. Chan, C. Lam, and F. G. Shin, Mechanisms of imprint effect on ferroelectric thin films, J. Appl. Phys. **98**, 024111 (2005).

[41] S. V. Kalinin, C. Y. Johnson, and D. A. Bonnell, Domain polarity and temperature induced potential inversion on the $BaTiO_3$ (100) surface, J. Appl. Phys. **91**, 3816 (2002).

[42] K. M. Rabe, C. H. Ahn, and J.-M. Triscone, *Physics of ferroelectrics: a modern perspective*, Vol. 105 (Springer, 2007) pp. 96–97.

[43] T. Qi, Y. H. Shin, K. L. Yeh, K. A. Nelson, and A. M. Rappe, Collective coherent control: Synchronization of polarization in ferroelectric $PbTiO_3$ by shaped THz fields, Phys. Rev. Lett. **102**, 247603 1 (2009).

[44] A. Ali, H. Madan, R. Misra, A. Agrawal, P. Schiffer, J. Boos, B. R. Bennett, and S. Datta, Experimental determination of quantum and centroid capacitance in arsenide–antimonide quantum-well mosfets incorporating nonparabolicity effect, IEEE Trans. Electron Devices **58**, 1397 (2011).

[45] O. G. Udalov, N. M. Chtchelkatchev, and I. S. Beloborodov, Proximity coupling of a granular film with a ferroelectric substrate and giant electroresistance effect, Phys. Rev. B **90**, 054201 (2014).

[46] C. Baeumer, D. Saldana-Greco, J. M. P. Martirez, A. M. Rappe, M. Shim, and L. W. Martin, Ferroelectrically driven spatial carrier density modulation in graphene, Nat. Comm. **6** (2015).

[47] X. Hong, A. Posadas, K. Zou, C. H. Ahn, and J. Zhu, High–mobility few–layer graphene field effect transistors fabricated on epitaxial ferroelectric gate oxides, Phys. Rev. Lett. **102**, 136808 (2009).

[48] X. Hong, J. Hoffman, A. Posadas, K. Zou, C. H. Ahn, and J. Zhu, Unusual resistance hysteresis in n–layer graphene field effect transistors fabricated on ferroelectric $Pb(Zr_{0.2}Ti_{0.8})O_3$, Appl. Phys. Lett. **97**, 033114 (2010).

[49] R. E. Cohen, Electronic structure studies of the differences in ferroelectric behaviour of $BaTiO_3$ and $PbTiO_3$, Ferroelectrics **136**, 65 (1992).